LETTER

doi:10.1038/nature12978

Structure-based programming of lymph-node targeting in molecular vaccines

Haipeng Liu[1,2,3], Kelly D. Moynihan[2,3], Yiran Zheng[2,3], Gregory L. Szeto[2,3], Adrienne V. Li[2,3], Bonnie Huang[2,3], Debra S. Van Egeren[4], Clara Park[2] & Darrell J. Irvine[1,2,3,5,6]

In cancer patients, visual identification of sentinel lymph nodes (LNs) is achieved by the injection of dyes that bind avidly to endogenous albumin, targeting these compounds to LNs, where they are efficiently filtered by resident phagocytes[1,2]. Here we translate this 'albumin hitchhiking' approach to molecular vaccines, through the synthesis of amphiphiles (amph-vaccines) comprising an antigen or adjuvant cargo linked to a lipophilic albumin-binding tail by a solubility-promoting polar polymer chain. Administration of structurally optimized CpG-DNA/peptide amph-vaccines in mice resulted in marked increases in LN accumulation and decreased systemic dissemination relative to their parent compounds, leading to 30-fold increases in T-cell priming and enhanced anti-tumour efficacy while greatly reducing systemic toxicity. Amph-vaccines provide a simple, broadly applicable strategy to simultaneously increase the potency and safety of subunit vaccines.

A major challenge in the development of subunit vaccines is the efficient delivery of antigen/adjuvant to secondary lymphoid organs, where immune responses are orchestrated[3,4]. Attempts to enhance vaccine delivery have included the use of depot-forming adjuvants[5] or nanoparticulate carriers that are preferentially internalized by antigen presenting cells (APCs)[4,6–12], but approaches that could use well-defined molecular conjugates would be attractive. Antigens conjugated to antibodies targeting dendritic cells reach these cells in the draining LNs but also drain into the systemic circulation and access APCs in distal tissues[13,14], which might promote tolerance unless inflammatory adjuvants are systemically co-administered. LN targeting is also required for cancer staging in sentinel LN mapping procedures, in which radioactive or coloured dyes are injected at tumour resection sites[1]. Compounds that bind avidly to serum albumin are particularly effective LN tracers[2]; albumin binding targets these molecules to lymphatics and draining LNs, where they accumulate in APCs[15,16]. Inspired by this strategy, we set out to create LN-targeting molecular vaccines designed to similarly 'hitchhike' on albumin to LNs. Exploiting albumin's role as a fatty acid transporter, we proposed that antigens/adjuvants modified with a lipophilic albumin-binding domain would accumulate in lymphoid organs after injection, through *in situ* complexation and transport with endogenous albumin. To develop this strategy, we studied model vaccines composed of peptide antigens and CpG DNAs, single-stranded oligonucleotides containing unmethylated cytosine-guanine motifs that bind Toll-like receptor 9 (TLR9) and serve as potent molecular adjuvants[17,18].

To identify an optimal albumin-binding domain that could be appended to either CpG or peptide antigens, we constructed a series of amphiphilic 20-base phosphorothioate (PS)-stabilized CpG oligonucleotides 5′-linked to lipophilic tails (amph-CpGs; Fig. 1a; for synthesis details see Supplementary Information). We first evaluated the interaction of fluorescein amidite (FAM)-labelled conjugates with serum proteins by size-exclusion chromatography (SEC; Fig. 1b). Fetal bovine serum (FBS) exhibited a major protein fraction eluting at 5.3 min in SEC that coincided with albumin (Extended Data Fig. 1a). The vast majority of mono-acyl-conjugated (C18-CpG) or cholesterol-conjugated (Cho-CpG) oligonucleotides eluted as monomers at 5.8 min in the presence or absence of serum, indicating a lack of interaction with albumin (Fig. 1b and Extended Data Fig. 1a). By contrast, diacyl lipid-conjugated CpGs (lipo-CpGs) in aqueous solution eluted as micelles (3.7 min), but, after incubation with serum, nearly 50% of the lipo-CpGs co-migrated with albumin (Fig. 1b). Biotinylated lipo-CpG (but not CpG) incubated with FBS and then captured with magnetic beads was found to pull down albumin, and lipo-CpG was efficiently captured by albumin-conjugated agarose (Extended Data Fig. 1b, c). Biolayer interferometry and spectroscopy measurements of fluorescence resonance energy transfer (FRET) between lipo-CpG and purified albumin further confirmed their molecular association in solution (Extended Data Fig. 1d, e).

We next characterized the *in vivo* trafficking of CpG conjugates. Amph-CpGs were injected subcutaneously in C57BL/6 mice, and 24 h later, draining LNs were excised intact for *in vivo* imaging system (IVIS) fluorescence imaging. C18- and Cho-CpG showed marginally increased uptake in LNs relative to unmodified CpG, reaching levels similar to CpG delivered by two prototypical vaccine vehicles known to enhance vaccine accumulation in LNs, incomplete Freund's adjuvant (IFA) or poly(ethylene glycol) (PEG)-coated liposomes[6] (Fig. 1c). By contrast, lipo-CpG accumulated eightfold more than soluble CpG (Fig. 1c). Over 7 days after injection, soluble CpG exhibited no LN accumulation above 0.3% of the injected dose at any time, whereas lipo-CpG accumulated for 3 days, giving a 12-fold greater area under the curve (AUC) for total LN exposure to CpG (Fig. 1d). LN accumulation was not dependent on TLR9-recognized CpG motifs, and was not due to increased nuclease resistance of lipid-modified PS-backbone CpGs (data not shown).

Our *in vitro* analysis indicated that lipo-CpG molecules equilibrated between micellar and albumin-bound forms in the presence of serum, making it unclear which state was responsible for LN targeting. However, injection of lipo-CpG pre-incubated for 5 h with freshly isolated 90 vol% mouse serum at 37 °C, conditions in which SEC showed the vast majority of the amphiphile co-migrated with albumin, led to essentially identical LN targeting compared with direct lipo-CpG injections (data not shown). To address this question further, we introduced poly-guanine repeats between the diacyl lipid and CpG sequence to lock the amphiphiles in the micellar state and block disassembly by albumin. G-quadruplex hydrogen bonding between adjacent oligonucleotide strands in lipo-G_n-CpG micelles containing four or more guanine repeats rendered the micelles stable in the presence of serum (Extended Data Fig. 2a–d). Labelled albumin did not co-migrate with stabilized micelles, as assessed by SEC (Extended Data Fig. 2e), suggesting that the amphiphiles do not interact with albumin as intact micelles. Despite forming micelles with similar sizes (Extended Data Fig. 2f), G-quartet-stabilized

[1]Department of Materials Science and Engineering, Massachusetts Institute of Technology, Cambridge, Massachusetts 02139, USA. [2]Department of Biological Engineering, Massachusetts Institute of Technology, Cambridge, Massachusetts 02139, USA. [3]Koch Institute for Integrative Cancer Research, Massachusetts Institute of Technology, Cambridge, Massachusetts 02139, USA. [4]Department of Biology, Massachusetts Institute of Technology, Cambridge, Massachusetts 02139, USA. [5]Ragon Institute of Massachusetts General Hospital, Massachusetts Institute of Technology, and Harvard, Cambridge, Massachusetts 02139, USA. [6]Howard Hughes Medical Institute, Chevy Chase, Maryland 20815, USA.

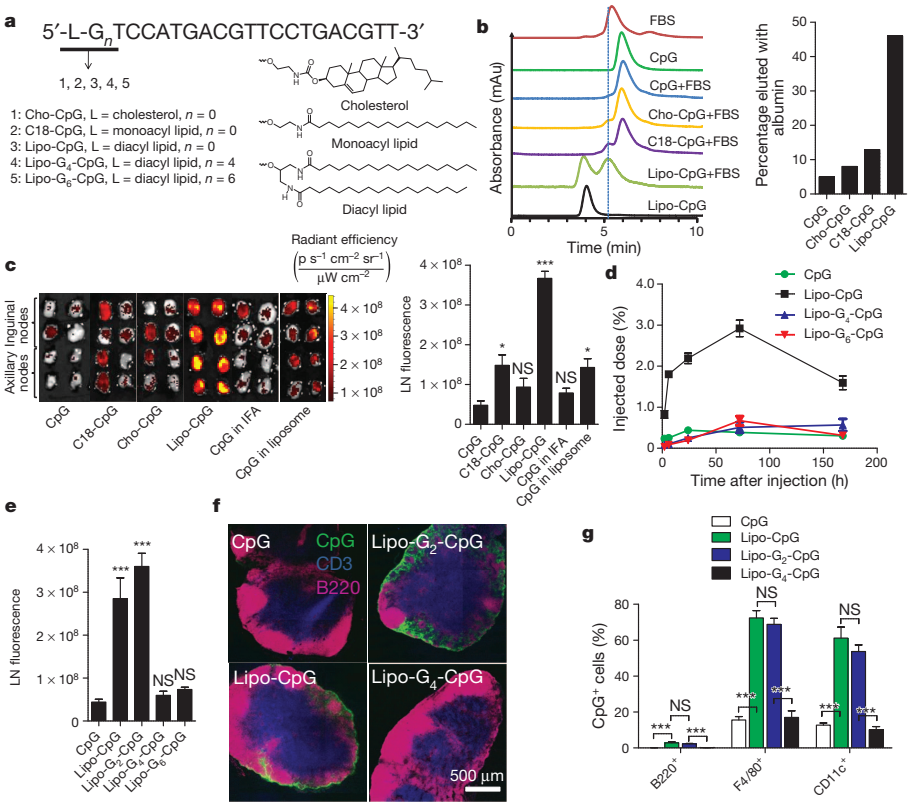

Figure 1 | Design of an LN-targeted molecular adjuvant. **a**, Structure of amph-CpGs. **b**, SEC of FAM-CpGs alone or after incubation with FBS for 2 h (left), and percentage CpG co-migrating with albumin peaks (right). Vertical dashed line provides a guide to the eye. **c**–**g**, IVIS fluorescence imaging of excised draining LNs from C57BL/6 mice ($n = 4$ LNs per group) injected with FAM-CpGs (3.3 nmol) in soluble form, emulsified in IFA, entrapped in liposomes, or as amphiphile conjugates. **c**, IVIS images and quantification from inguinal and axillary nodes at 24 h. **d**, CpG accumulation in draining LNs. **e**, IVIS quantification of CpG in LNs 24 h after injection of G-quadruplex-forming Lipo-G$_n$-CpGs. **f**, Immunohistochemistry of inguinal LNs 24 h after injection (CD3, blue; B220, pink; CpG, green). **g**, LN CpG$^+$ cells determined by flow cytometry at 24 h. ***$P < 0.001$, **$P < 0.01$, *$P < 0.05$ compared with soluble CpG by one-way analysis of variance (ANOVA) with Bonferroni post-test. Data represent mean ± standard error of the mean (s.e.m.) of 2–3 independent experiments. NS, not significant.

lipo-G$_4$-CpG or lipo-G$_6$-CpG micelles exhibited poor LN accumulation after injection compared with albumin-binding lipo-CpG and lipo-G$_2$-CpG (Fig. 1d, e). A possible explanation is that amplification of nonspecific matrix binding by the PS-DNA backbones[19,20] in the multivalent micellar form irreversibly trapped the stabilized micelles at the injection site. Histological sections of draining LNs showed little detectable CpG or lipo-G$_4$-CpG, whereas albumin-binding lipo-CpG and lipo-G$_2$-CpG accumulated in the subcapsular sinus and interfollicular areas (Fig. 1f). LN-accumulating amphiphiles were associated with F4/80$^+$ macrophages and CD11c$^+$ dendritic cells, with only a minor contribution from skin-derived CD207$^+$ dendritic cells (Fig. 1g and Extended Data Fig. 3). If albumin hitchhiking mediates LN targeting, then covalent conjugation of oligonucleotides to albumin should also enhance LN accumulation. We found that injection of CpG conjugated to mouse serum albumin (MSA) led to slightly lower oligonucleotide uptake in LNs than lipo-CpG, but much greater accumulation than soluble CpG (Extended Data Fig. 4). Altogether, these data suggest that efficient LN delivery of CpG oligonucleotides conjugated to lipophilic tails is enhanced by partitioning of oligonucleotides from micelles into a serum albumin-bound state.

To identify potential differences in the function of CpG versus optimally LN-targeted lipo-G$_2$-CpG beyond altered biodistribution, we assessed several aspects of CpG bioactivity *in vitro*: lipo-G$_2$-CpG was internalized by dendritic cells into endolysosomes in a pattern indistinguishable from CpG in confocal microscopy, albeit to twofold higher levels (Extended Data Fig. 5a, b). Lipo-G$_2$-CpG did not activate the lipid-binding receptor TLR2 in reporter cells, but both free CpG and amph-CpG activated RAW macrophages bearing a NF-κB reporter in a CpG sequence-specific manner (Extended Data Fig. 5c, d). When dendritic cells were activated with CpG or lipo-G$_2$-CpG and pulsed with OVA protein to test cross-presentation of antigen to OT-I (OVA-specific) T-cells, dendritic cell activation by soluble or amphiphile-CpG led to similar T-cell proliferation (Extended Data Fig. 5e). Thus, lipid modification of CpG increased uptake in the presence of serum but did not otherwise greatly alter the bioactivity of CpG.

To determine the impact of LN targeting on the immune response, we immunized mice with ovalbumin protein (OVA) mixed with unmodified CpG, Cho-CpG, CpG emulsified in IFA or lipo-G$_n$-CpGs ($n = 0$, 2, 4, 6). OVA (which has only 13% sequence identity with albumin) showed minimal association with lipo-CpGs (data not shown) and thus these vaccinations assessed the impact of LN targeting of the adjuvant only, relying on normal lymphatic drainage of the OVA antigen. Lipo-G$_n$-CpG-adjuvanted vaccines primed significantly increased frequencies of antigen-specific, cytokine-producing CD8$^+$ T cells compared with unmodified CpG, Cho-CpG or CpG in IFA, but the strongest responses (up to 32-fold greater than unmodified CpG) were elicited by lipo-CpG and lipo-G$_2$-CpG (Fig. 2a, b and Extended Data Fig. 6a, b). Notably, the magnitude of the T-cell response was strongly correlated with LN accumulation of CpG (Fig. 2c). Lipo-CpG also modestly increased antibody responses by approximately threefold and enhanced CD8$^+$ T-cell responses to the model HIV antigen simian immunodeficiency virus (SIV) Gag (Extended Data Fig. 6c, d). Importantly, no antibodies against albumin were detected for any of the amph-CpG vaccines (Extended Data Fig. 6e, f and data not shown). Control immunizations with non-TLR agonist lipo-GpC or diacyl-PEG conjugates (lipo-PEG) mixed with OVA were ineffective and amph-CpG responses were identical in *Tlr2*$^{-/-}$ mice (Extended Data Fig. 6g, h), ruling out a direct adjuvant effect of the diacyl lipid tail. CpG that is not captured in local LNs drains to the systemic circulation, leading to systemic inflammatory toxicities[21]. Despite lymphadenopathy of draining LNs, indicating local activity, repeated injections of lipo-CpGs showed greatly reduced systemic inflammation relative to free CpG (Fig. 2d, e and Extended Data Fig. 7a, b). Although further work will be needed to determine any potential autoimmune toxicities related to LN targeting of CpG[18], these results suggest that the LN targeting achieved by amph-CpGs greatly enhances the potency of this molecular adjuvant while simultaneously lowering acute systemic side effects.

Synthesis of lipo-CpG is straightforward owing to the solubility imparted by the long polar oligonucleotide block, but, depending on the amino acid sequence, lipidated polypeptides can be essentially insoluble[22].

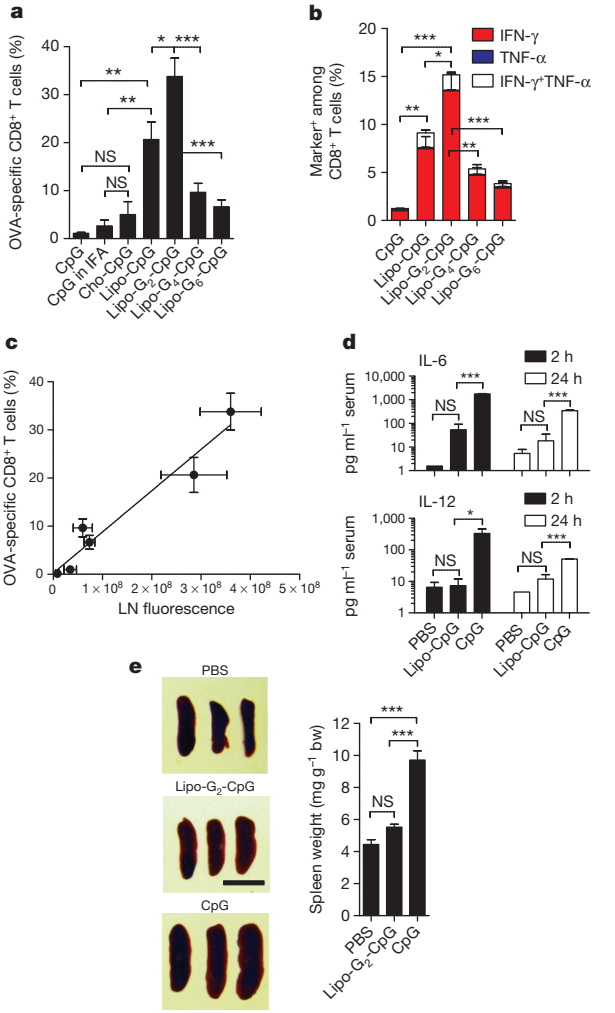

Figure 2 | LN targeting enhances potency while reducing systemic toxicity of CpG. **a**–**c**, C57BL/6 mice ($n = 4$–8 per group) were immunized with OVA (10 μg) plus CpG (1.24 nmol) on day 0 and day 14; shown are SIINFEKL tetramer (**a**) and intracellular cytokine staining (**b**) on peripheral blood at day 20. **c**, LN CpG fluorescence correlation with T-cell response. **d**, Serum cytokines after injection ($n = 3$ per group) of 6.2 nmol CpG. **e**, Splenomegaly ($n = 3$ per group) assessed on day 6 after three injections of CpG. bw, body weight. Scale bar, 1 cm. $^{***}P < 0.001$, $^{**}P < 0.01$, $^{*}P < 0.05$ by one-way ANOVA with Bonferroni post-test. Data show mean ± s.e.m. of 2–4 independent experiments. NS, not significant.

To generalize this LN targeting strategy to antigens and other potential vaccine components, we synthesized peptides linked to a diacyl lipid tail via a PEG block chosen to promote conjugate solubility (amph-peptides; Fig. 3a). Amph-peptides and lipo-PEGs in water form micelles, but these amphiphiles can also insert their diacyl tails into cell membranes. We found that lipo-PEG amphiphiles with short PEG blocks exhibited preferential plasma membrane insertion when incubated with cells in the presence of albumin *in vitro* (Fig. 3b and Extended Data Fig. 8a, b), which might limit transit to LNs on albumin *in vivo*. However, increasing the polar block to 48 ethylene glycol units yielded amphiphiles that partitioned preferentially into solution while retaining albumin binding (Fig. 3b and Extended Data Fig. 8c), consistent with previous studies[23]. This *in vitro* partitioning directly predicted *in vivo* draining patterns, as lipo-PEG-FAM amphiphiles injected subcutaneously showed increasing LN accumulation with increasing PEG block length (Fig. 3c). Although optimal immunostimulatory CpGs are ~20 bases, an analogous trend was observed for DNA amphiphiles as a function of oligonucleotide length (Extended Data Fig. 8d, e). Like amph-CpGs, the structure of the hydrophobic block was also important; whereas lipo-PEG amphiphiles with long diacyl tails (≥16 carbons, which exhibit a high affinity for albumin[24]) showed intense LN accumulation, shorter lipid tails with low affinity for albumin showed low LN accumulation (Fig. 3d). On the basis of these findings establishing design rules for efficient targeting of lipo-PEG amphiphiles to LNs, we conjugated peptide antigens to 1,2-distearoyl-*sn*-glycero-3-phosphoethanolamine-*N*-PEG (DSPE-PEG 2 kDa) to generate amph-peptides for vaccination studies (Extended Data Fig. 9a).

To test the potency of combined antigen and adjuvant targeting to LNs, we prepared amph-peptide (DSPE-PEG-peptide) conjugates of a model HIV antigen (AL11 epitope from SIV Gag)[25], the tumour-associated self-antigen Trp2 from melanoma[26], and a peptide derived from the human papillomavirus (HPV)-derived cervical cancer antigen E7 (ref. 27). Amph-peptides accumulated efficiently in LNs (Extended Data Fig. 9b, c). C57BL/6 mice immunized with amph-peptides and amph-CpG (lipo-G_2-CpG) showed markedly increased expansion of antigen-specific, cytokine-producing $CD8^+$ T-cells and enhanced cytolytic activity relative to unmodified peptide/CpG immunizations (Fig. 4a–c). To test whether amph-vaccine delivery enhances the protective efficacy of peptide vaccines, animals bearing established TC-1 tumours (expressing the E7 oncoprotein from HPV) or B16F10 melanomas were vaccinated. Amph-vaccines triggered sustained regression of large TC-1 tumours that were only modestly affected by soluble vaccines (Fig. 4d) and slowed the growth of melanoma tumours, in which a traditional soluble vaccine had no effect (Fig. 4e). In addition to enhancing the effectiveness of optimal T-cell epitopes, synthetic 'long peptide' antigens[28] also exhibited enhanced immunogenicity when delivered as amph-peptides (Extended Data Fig. 10a–e). This result is of particular interest because a finite pool of long sequences permits peptide vaccines to provide effective coverage of epitopes across the diverse haplotypes of a given target patient population. Amphiphile-long peptides were also approximately tenfold more potent than soluble peptides when combined with non-CpG, non-LN-targeted alternative TLR adjuvants (Extended Data Fig. 10f), showing that CpG is not required for an enhanced response to LN-targeted peptides.

Altogether, the results presented here define design rules for amphiphile conjugates as a general strategy to enhance the potency and safety

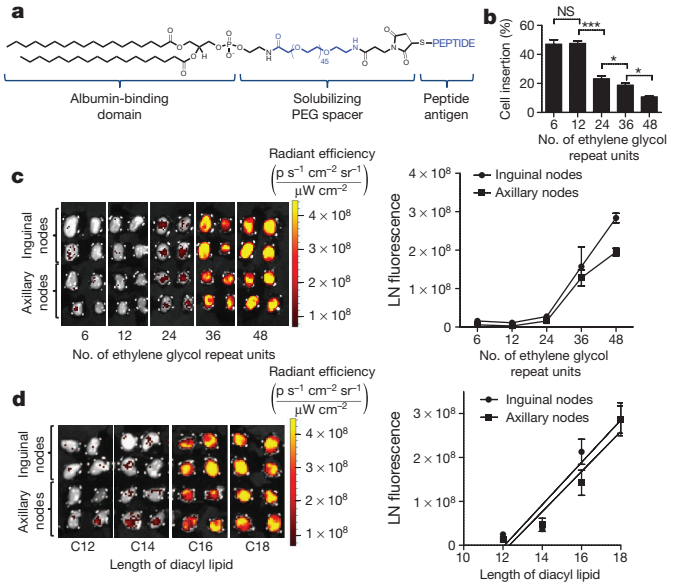

Figure 3 | Design of LN-targeted amph-peptides. **a**, Structure of amph-peptides. **b**, Amph-PEG-fluorescein insertion into cell membranes quantified by fluorescence spectroscopy after 1 h incubation with splenocytes in the presence of 100 μM albumin. **c**, **d**, C57BL/6 mice ($n = 4$ LNs per group) were injected with fluorescent amph-PEGs with varying PEG lengths (fixed C18 diacyl lipid tails; **c**) or lipid tail lengths (fixed PEG length 48 EG units; **d**); draining LNs were excised and imaged by IVIS after 24 h. $^{***}P < 0.001$, $^{**}P < 0.01$, $^{*}P < 0.05$ by one-way ANOVA with Bonferroni post-test. Data represent mean ± s.e.m. of two independent experiments. NS, not significant.

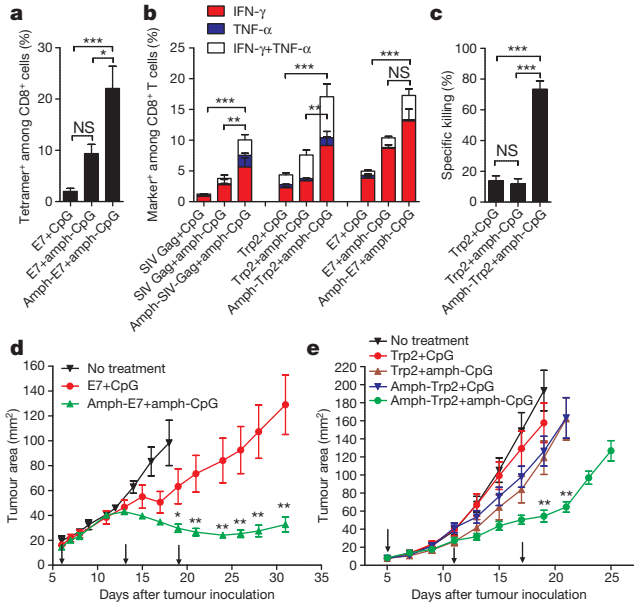

Figure 4 | Amph-vaccines maximize the immunogenicity and therapeutic efficacy of polypeptide vaccines. a–c, C57BL/6 mice ($n = 3$–4 per group) were immunized with SIV Gag, Trp2, or E7 peptides (10 μg) plus CpG (1.24 nmol) on day 0 and day 14; shown are tetramer-positive $CD8^+$ T-cells (**a**) and intracellular cytokine production (**b**) in peripheral blood on day 20. **c**, Trp2-specific cytotoxicity measured using an *in vivo* killing assay on day 21. **d**, **e**, Tumour growth in C57BL/6 mice ($n = 8$ per group) inoculated with 3×10^5 TC-1 (**d**) or B16F10 (**e**) tumour cells and vaccinated with CpG plus E7 peptide or Trp2 peptide (10 μg prime, 20 μg boost), respectively, on days indicated by arrows. Statistically significant differences between soluble and amph-vaccines are indicated by asterisks: $***P < 0.001$, $**P < 0.01$, $*P < 0.05$ by one-way ANOVA with Bonferroni post-test. Data show mean ± s.e.m. of 2–4 independent experiments. NS, not significant.

of LN-active compounds, an approach that may be applicable to a broad range of immunomodulatory therapeutics and imaging agents. These findings also have implications for how the immune system may survey lipophilic antigens. Further work will be needed to determine whether albumin binding is functionally critical, or alternatively whether other rare serum components may have a role in the observed LN targeting.

METHODS SUMMARY

Synthesis of vaccine amphiphiles. Oligonucleotide amphiphiles were synthesized using an ABI 394 synthesizer on a 1.0 μmol scale. All lipophilic phosphoramidites were conjugated as a final 'base' on the 5′ end of oligonucleotides[19]. Antigen amphiphiles were synthesized by reacting N-terminal cysteine-modified peptides with maleimide-PEG_{2000}-DSPE in dimethyl formamide.

Immunizations. Six-to-eight week old C57BL/6 mice (female, Jackson Laboratory) were immunized with 10 μg of antigen mixed with 1.24 nmol CpG adjuvant in 100 μl of PBS subcutaneously at the base of the tail. All procedures were performed under an IUCAC-approved animal protocol in accordance with the guidelines for animal care in a Massachusetts Institute of Technology animal facility inspected by the US Department of Agriculture.

Online Content Any additional Methods, Extended Data display items and Source Data are available in the online version of the paper; references unique to these sections appear only in the online paper.

Received 20 May; accepted 30 December 2013.
Published online 16 February 2014.

1. Salhab, M., Patani, N. & Mokbel, K. Sentinel lymph node micrometastasis in human breast cancer: an update. *Surg. Oncol.* **20,** e195–e206 (2011).
2. Tsopelas, C. & Sutton, R. Why certain dyes are useful for localizing the sentinel lymph node. *J. Nucl. Med.* **43,** 1377–1382 (2002).
3. Johansen, P., Mohanan, D., Martínez-Gómez, J. M., Kündig, T. M. & Gander, B. Lymphogeographical concepts in vaccine delivery. *J. Control. Release* **148,** 56–62 (2010).
4. Moon, J. J., Huang, B. & Irvine, D. J. Engineering nano- and microparticles to tune immunity. *Adv. Mater.* **24,** 3724–3746 (2012).
5. Gupta, R. K. Aluminum compounds as vaccine adjuvants. *Adv. Drug Deliv. Rev.* **32,** 155–172 (1998).
6. Bachmann, M. F. & Jennings, G. T. Vaccine delivery: a matter of size, geometry, kinetics and molecular patterns. *Nature Rev. Immunol.* **10,** 787–796 (2010).
7. Hubbell, J. A., Thomas, S. N. & Swartz, M. A. Materials engineering for immunomodulation. *Nature* **462,** 449–460 (2009).
8. De Temmerman, M. L. *et al.* Particulate vaccines: on the quest for optimal delivery and immune response. *Drug Discov. Today* **16,** 569–582 (2011).
9. Pal, I. & Ramsey, J. D. The role of the lymphatic system in vaccine trafficking and immune response. *Adv. Drug Deliv. Rev.* **63,** 909–922 (2011).
10. Reddy, S. T. *et al.* Exploiting lymphatic transport and complement activation in nanoparticle vaccines. *Nature Biotechnol.* **25,** 1159–1164 (2007).
11. St John, A. L., Chan, C. Y., Staats, H. F., Leong, K. W. & Abraham, N. A. Synthetic mast-cell granules as adjuvants to promote and polarize immunity in lymph nodes. *Nature Mater.* **11,** 250–257 (2012).
12. Trubetskoy, V. S. & Torchilin, V. P. Use of polyoxyethylene-lipid conjugates as long-circulating carriers for delivery of therapeutic and diagnostic agents. *Adv. Drug Deliv. Rev.* **16,** 311–320 (1995).
13. Keler, T., He, L., Ramakrishna, V. & Champion, B. Antibody-targeted vaccines. *Oncogene* **26,** 3758–3767 (2007).
14. Tenbusch, M. *et al.* Immunogenicity of DNA vaccines encoding simian immunodeficiency virus antigen targeted to dendritic cells in rhesus macaques. *PLoS ONE* **7,** e39038 (2012).
15. Faries, M. B. *et al.* Active macromolecule uptake by lymph node antigen-presenting cells: a novel mechanism in determining sentinel lymph node status. *Ann. Surg. Oncol.* **7,** 98–105 (2000).
16. Schaafsma, B. E. *et al.* The clinical use of indocyanine green as a near-infrared fluorescent contrast agent for image-guided oncologic surgery. *J. Surg. Oncol.* **104,** 323–332 (2011).
17. Vollmer, J. & Krieg, A. M. Immunotherapeutic applications of CpG oligodeoxynucleotide TLR9 agonists. *Adv. Drug Deliv. Rev.* **61,** 195–204 (2009).
18. Bode, C., Zhao, G., Steinhagen, F., Kinjo, T. & Klinman, D. M. CpG DNA as a vaccine adjuvant. *Expert Rev. Vaccines* **10,** 499–511 (2011).
19. Liu, H., Kwong, B. & Irvine, D. J. Membrane anchored immunostimulatory oligonucleotides for *in vivo* cell modification and localized immunotherapy. *Angew. Chem. Int. Ed. Engl.* **50,** 7052–7055 (2011).
20. Krieg, A. M. & Stein, C. A. Phosphorothioate oligodeoxynucleotides: antisense or anti-protein? *Antisense Res. Dev.* **5,** 241 (1995).
21. Bourquin, C. *et al.* Targeting CpG oligonucleotides to the lymph node by nanoparticles elicits efficient antitumoral immunity. *J. Immunol.* **181,** 2990–2998 (2008).
22. Zeng, W., Ghosh, S., Lau, Y. F., Brown, L. E. & Jackson, D. C. Highly immunogenic and totally synthetic lipopeptides as self-adjuvanting immunocontraceptive vaccines. *J. Immunol.* **169,** 4905–4912 (2002).
23. Kastantin, M. *et al.* Thermodynamic and kinetic stability of DSPE-PEG(2000) micelles in the presence of bovine serum albumin. *J. Phys. Chem. B* **114,** 12632–12640 (2010).
24. Peters, T. *All About Albumin: Biochemistry, Genetics, and Medical Applications* (Academic, 1995).
25. Barouch, D. H. *et al.* Immunogenicity of recombinant adenovirus serotype 35 vaccine in the presence of pre-existing anti-Ad5 immunity. *J. Immunol.* **172,** 6290–6297 (2004).
26. Schreurs, M. W. *et al.* Dendritic cells break tolerance and induce protective immunity against a melanocyte differentiation antigen in an autologous melanoma model. *Cancer Res.* **60,** 6995–7001 (2000).
27. Feltkamp, M. C. *et al.* Vaccination with cytotoxic T lymphocyte epitope-containing peptide protects against a tumor induced by human papillomavirus type 16-transformed cells. *Eur. J. Immunol.* **23,** 2242–2249 (1993).
28. Kenter, G. G. *et al.* Vaccination against HPV-16 oncoproteins for vulvar intraepithelial neoplasia. *N. Engl. J. Med.* **361,** 1838–1847 (2009).

Supplementary Information is available in the online version of the paper.

Acknowledgements This work was supported in part by the Koch Institute Support (core) grant P30-CA14051 from the National Cancer Institute, the National Institutes of Health (grants AI091693, AI104715 and AI095109), the Department of Defense (W911NF-13-D-0001 and W911NF-07-D-0004, T.O. 8) and the Ragon Institute of Massachusetts General Hospital, the Massachusetts Institute of Technology and Harvard. D.J.I. is an investigator of the Howard Hughes Medical Institute. We thank T. C. Wu for kindly providing the TC-1 tumour cells. We thank the Koch Institute Swanson Biotechnology Center for technical support, specifically the applied therapeutics and whole animal imaging core facility, histology and flow cytometry core facility. The authors acknowledge the service to the MIT community of the late Sean Collier.

Author Contributions H.L. designed and performed most experiments and analysed the data, and wrote the manuscript; Y.Z. carried out tumour therapy experiments and analysed the data. K.D.M. carried out *in vitro* bioactivity studies of CpG, biolayer interferometry binding studies and *in vivo* immunizations of SIV Gag and analysed the data. A.V.L. and B.H. assisted in tetramer/*in vivo* cytotoxicity assays and contributed experimental suggestions. G.L.S. assisted with optimization of proinflamatory cytokine assays and helped *in vitro* bioactivity studies of CpG. G.L.S., C.P. and D.S.V.E. contributed to *in vitro* T-cell proliferation assays. D.J.I. supervised all experiments and wrote the manuscript.

Author Information Reprints and permissions information is available at www.nature.com/reprints. The authors declare competing financial interests: details are available in the online version of the paper. Readers are welcome to comment on the online version of the paper. Correspondence and requests for materials should be addressed to D.J.I. (djirvine@mit.edu).

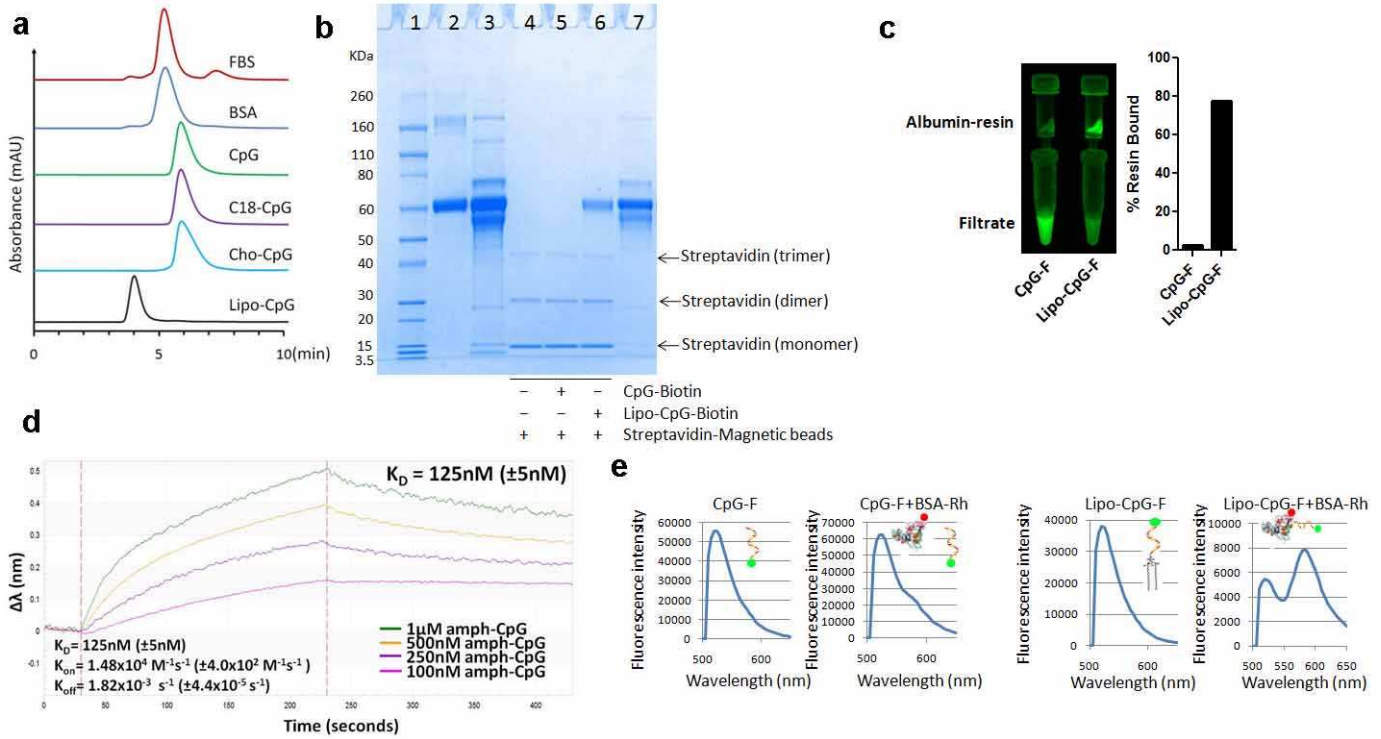

Extended Data Figure 1 | Interaction between albumin and amph-CpGs. **a**, SEC of FBS, albumin and fluorescein-labelled amph-CpGs. FBS and bovine serum albumin (BSA) were monitored using absorptions at 280 nm, whereas CpG oligonucleotides were monitored at 480 nm (fluorescein peak). **b**, Lipo-CpG, but not CpG, interacts with serum albumin as shown by SDS–polyacrylamide gel electrophoresis (SDS–PAGE) after protein pull-down assays: FBS was incubated with 3′-biotin-labelled CpG (CpG-biotin), lipo-CpG (lipo-CpG-biotin) or PBS for 1 h at 37 °C. Streptavidin-conjugated magnetic beads were added to capture biotinylated CpGs and any associated proteins, separated by a magnet, boiled to release bound CpG/proteins, and subjected to SDS–PAGE analysis. Lane 1: protein MW ladder; lane 2: purified BSA; lane 3: FBS (100× dilution, 10 μl loading); lane 4: pull-down control, FBS incubated with streptavidin-magnetic beads; lane 5: pull-down with CpG-biotin, FBS was incubated with CpG-biotin and streptavidin magnetic beads; lane 6: pull-down with lipo-CpG-biotin, FBS incubated with lipo-CpG-biotin and streptavidin magnetic beads; lane 7: FBS (100× dilution, 5 μl loading). **c**, Fluorescein-labelled CpG or lipo-CpG was incubated with albumin-conjugated agarose resin for 1 h at 37 °C, and the resin was separated by filtration. The filtrate and recovered agarose were visualized by a gel imager and quantified by fluorescence measurements. **d**, Bio-layer interferometry measurements of lipo-CpG and CpG binding to immobilized BSA. Albumin-conjugated BLI probes were immersed in solutions of lipo-CpG, and wavelength shifts ($\Delta\lambda$) of the interferometry pattern association and dissociation curves were followed over time to determine affinity constants of binding at 25 °C. Shown are apparent k_{on}, k_{off} and K_D values from fits to the data. **e**, FRET between FAM-labelled lipo-CpG and rhodamine-conjugated albumin (BSA-Rh) assessed by fluorescence spectroscopy. CpG-F or lipo-CpG-F (1.65 μM) alone or mixed with BSA-Rh (1.5 μM) in PBS were excited at 488 nm and emission was recorded from 500–650 nm.

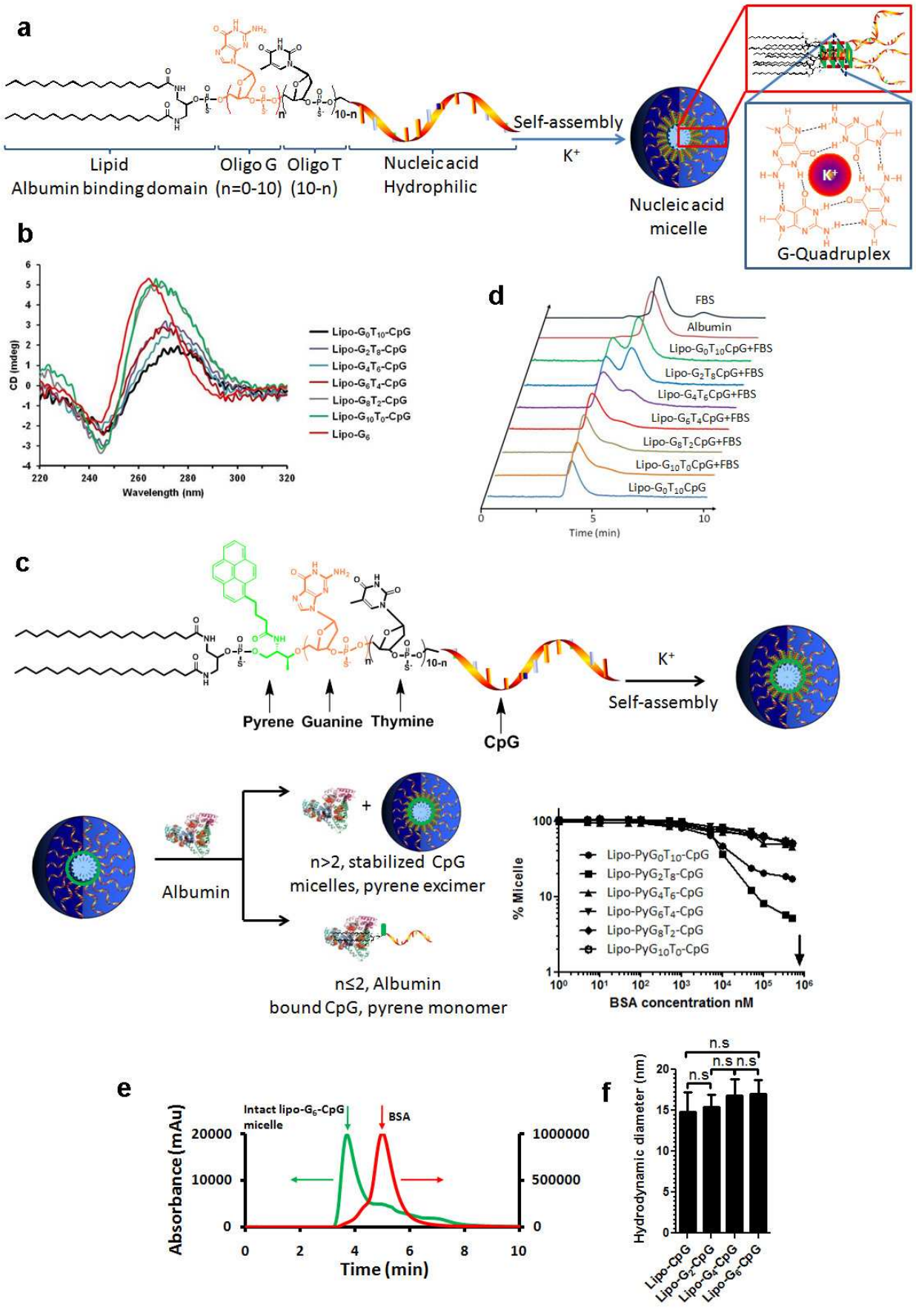

Extended Data Figure 2 | Construction and characterization of G-quadruplex-stabilized CpG adjuvants. **a**, G-quadruplex-stabilized CpG micelles are self-assembled from amphiphiles composed of three distinct segments: an immunostimulatory CpG sequence, a central repeat block containing $n = 1–10$ G-quartet-forming guanines followed by $(10 - n)$ non-interacting thymidines, and a diacyl lipid tail. In aqueous solutions, these amphiphiles self-assembled into three-dimensional spherical micelles with a CpG corona and a lipid core. In the presence of K^+, neighbouring guanine repeats in the oligonucleotide corona form G-quadruplex structures via Hoogsteen hydrogen bonds and stabilize the micelle structure. The stability of the oligonucleotide micelles in the presence of serum was programmed by altering the length of the guanine repeat. **b**, Parallel G-quartet formation among DNA strands within the micelles was detected by circular dichroism (CD) spectroscopy, as manifested by the shifting of positive peaks from 278 nm towards 262 nm and troughs at 245 nm as the number of guanines in the structure increased. **c**, Pyrene excimer fluorescence was used to assay the stabilities of G-quadruplex micelles in the presence of albumin: pyrene dye incorporated in stabilized CpG micelles ($n > 2$) retained excimer fluorescence in the presence of high concentrations of albumin. By contrast, albumin binds to the lipid moiety of unstabilized micelles ($n \leq 2$) and disrupts the micelle structures, leading to loss of excimer fluorescence in an albumin-concentration-dependent manner as the protein disrupts the micelles into albumin-bound unimers. Shown below the schematic is the fraction of amph-CpG remaining in the micellar state as a function of albumin concentration as reported by excimer fluorescence. Arrow indicates the plasma concentration of albumin. **d**, Stability profiles of G-quadruplex CpG micelles as measured by SEC in the presence of FBS. Fluorescein-labelled CpG micelles were incubated with 20% FBS in PBS in the presence of 10 mM Mg^{2+} and 20 mM K^+ at 37 °C for 2 h, then analysed by SEC. FBS and BSA were monitored using absorptions at 280 nm, whereas lipo-G_n-CpG amphiphiles were monitored at 480 nm (fluorescein peak). Lipo-G_n-CpG with $n = 0$ or 2 partitioned to co-migrate with albumin, whereas amphiphiles with $n > 2$ showed increasing fractions of the amphiphiles migrating as intact micelles in the presence of serum with increasing n. **e**, Fluorescein-labelled lipo-G_6-CpG (5 μM) and Alexa Fluor 647-labelled BSA (5 μM) were incubated for 2 h at 37 °C in PBS plus 20 mM KCl, and then analysed by SEC. Spectra were monitored at 480 nm (ODN channel, green line, fluorescein) and 640 nm (protein channel, red line, Alexa Fluor 647). The majority of BSA and CpG micellar aggregates eluted separately. **f**, Size of amph-CpG micelles as determined by dynamic light scattering. All data are mean ± s.e.m. Statistical analysis was performed by one-way ANOVA with Bonferroni post-tests.

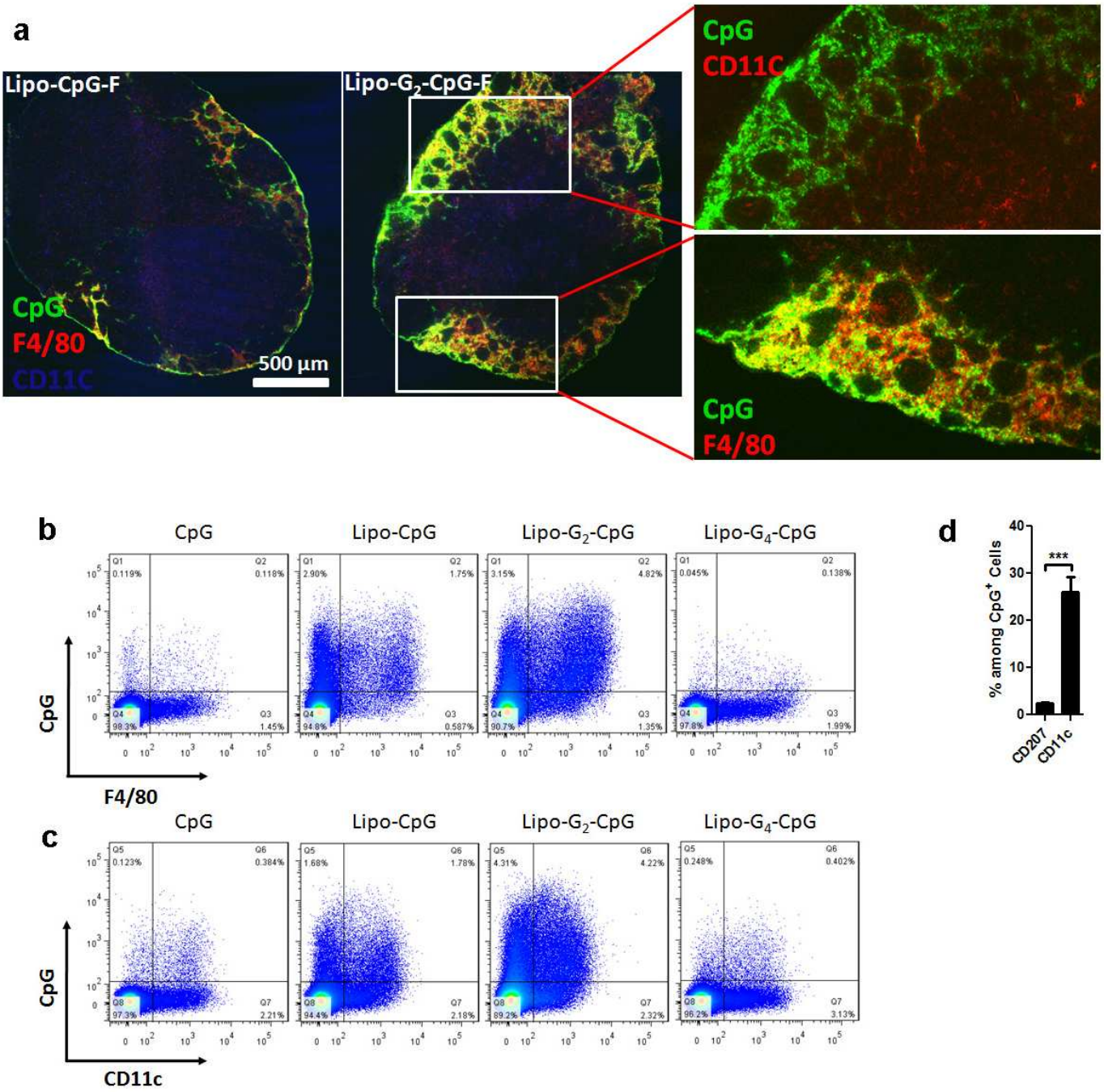

Extended Data Figure 3 | LN localization of amph-CpGs with macrophages and dendritic cells. **a**, Immunofluorescent images of inguinal LN section 24 h after injection of 3.3 nmol lipo-CpG or lipo-G_2-CpG, showing dendritic cells (CD11c, blue), macrophages (F4/80, red) and CpG (green). **b**–**d**, Mice ($n = 3$ per group) were injected subcutaneously with 3.3 nmol of fluorescein-labelled CpG formulations. After 24 h, LNs were digested and LN cells stained with 4′,6-diamidino-2-phenylindole (DAPI) and antibodies against F4/80, CD11c and CD207. **b**, **c**, Shown are representative flow cytometry plots of F4/80 staining (**b**) and CD11c staining (**c**) versus CpG fluorescence in viable ($DAPI^-$) cells. **d**, percentages of CpG^+ cells in the LNs determined by flow cytometry at 24 h. $***P < 0.001$; all data are mean ± s.e.m. Statistical analysis was performed by unpaired Student's *t*-test.

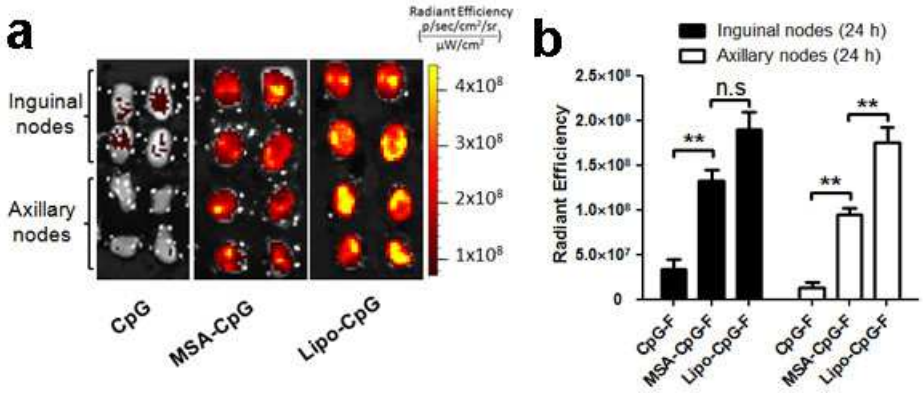

Extended Data Figure 4 | CpG-albumin conjugates accumulate in LNs. **a**, **b**, C57BL/6 mice ($n = 4$ LNs per group) were injected subcutaneously at the tail base with 3.3 nmol fluorescein-labelled free CpG, mouse albumin-CpG conjugates (MSA-CpG) or lipo-CpG. Inguinal LNs and axillary LNs were isolated 24 h after injection and imaged (**a**) and quantified (**b**) by IVIS optical imaging. All data are mean ± s.e.m. $^{**}P < 0.01$ by one-way ANOVA with Bonferroni post-test.

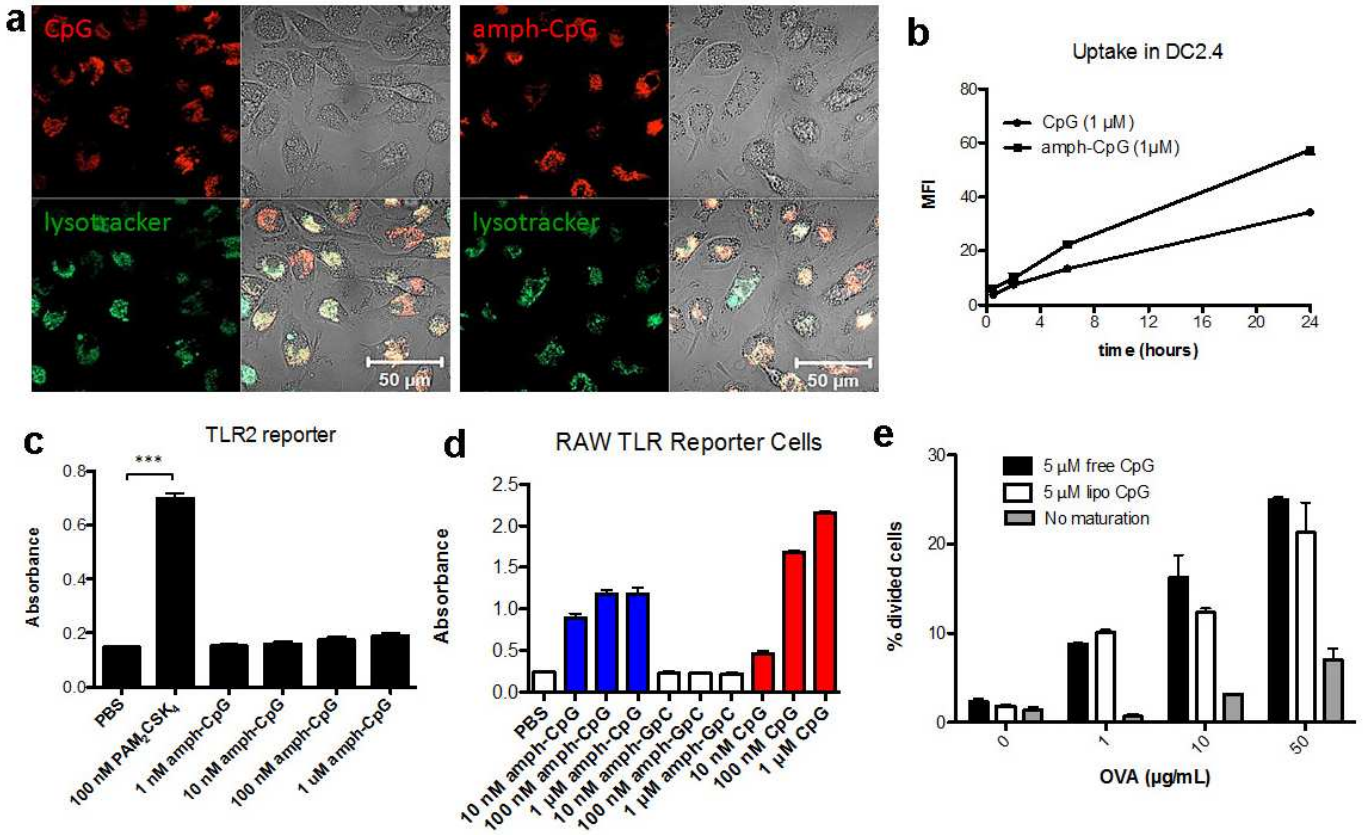

Extended Data Figure 5 | *In vitro* characterization of amph-CpG. **a**, Rhodamine-labelled CpG or amph-CpG (1 µM) was incubated with murine bone-marrow-derived dendritic cells at 37 °C for 4 h with LysoTracker (Life Technologies) and imaged using a Zeiss LSM 510 confocal microscope. **b**, Rhodamine-labelled CpG or amph-CpG (1 µM) was incubated for 30 min, 2 h, 6 h and 24 h with the murine dendritic cell line DC2.4. Cells were stained with DAPI and uptake was quantified by flow cytometry using the mean fluorescence intensity (MFI) of viable ($DAPI^-$) cells. **c**, Amph-CpG or PAM_2CSK_4 (a strong TLR2 agonist) was incubated for 24 h with the InvivoGen HEK-Blue murine TLR2 reporter cell line, a secreted embryonic alkaline phosphatase (SEAP) reporter system. SEAP levels were quantified by incubating supernatant with QuantiBlue substrate for 1 h and reading absorption at 620 nm. **d**, Amph-CpG, CpG or control amph-GpC (1 µM) were incubated with InvivoGen RAW-Blue mouse macrophage reporter cells, which secrete SEAP upon TLR, NOD or Dectin-1 stimulation. SEAP levels were quantified by incubating supernatant with QuantiBlue substrate for 1 h and reading absorption at 620 nm. **e**, Bone-marrow-derived immature dendritic cells were incubated overnight with indicated concentrations of OVA and maturation stimuli (or medium alone). Dendritic cells were washed three times with PBS and 30,000 CFSE-labelled OT-I $CD8^+$ T cells were then added to each well. Cells were collected after 2 days of co-culture, and stained and gated for $DAPI^-$ (viable) $CD8^+$ T cells using Flowjo v.7.6.5 (Treestar). The extent of proliferation was quantified by determining the percentage of cells that had undergone division by determining the percentage of viable $CD8^+$ T cells that had diluted CFSE using T cells alone as a control for the no division/dilution peak. Shown are mean ± s.e.m. **b**–**d**, $***P < 0.001$ by one-way ANOVA with Bonferroni post-test. Bars in **e** represent medians and whiskers represent range ($n = 2$ wells per condition).

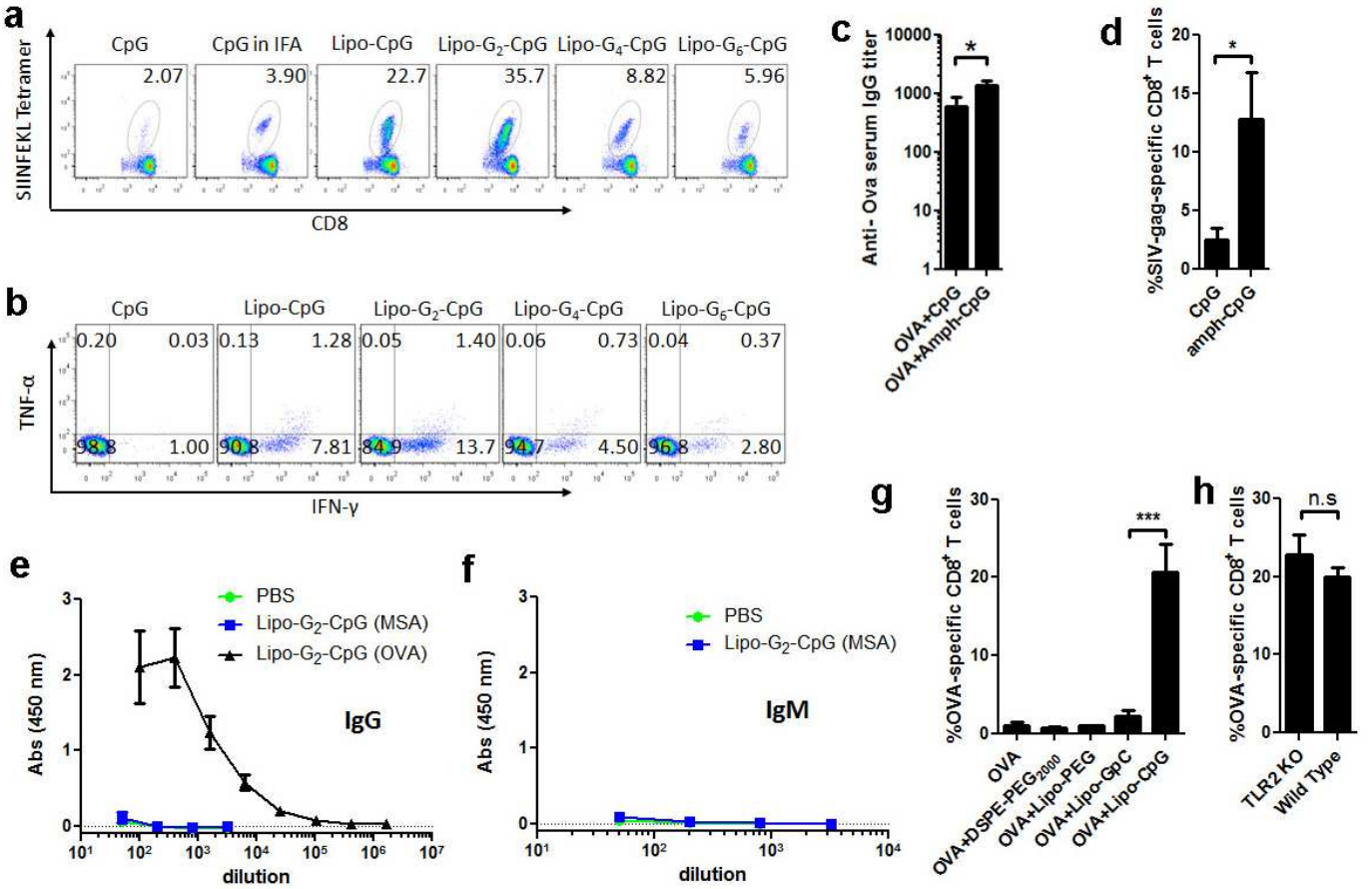

Extended Data Figure 6 | Albumin-binding lipo-CpGs elicit robust expansion of antigen-specific CD8$^+$ T-cells when combined with soluble protein. **a**–**h**, Groups of C57BL/6 mice ($n = 4$–8 per group) were immunized subcutaneously on day 0 and day 14 with 10 μg OVA and 1.24 nmol CpG formulations as indicated. Six days after the final immunization, mice were bled and peripheral blood mononuclear cells were evaluated by SIINFEKL-tetramer staining and intracellular cytokine staining. **a**, Representative flow cytometric dot plots of H-2K^b/SIINFEKL tetramer staining of CD8$^+$ cells. **b**, Representative flow dot plots of intracellular staining on CD8$^+$ cells for IFN-γ and TNF-α after 6 h *ex vivo* restimulation with SIINFEKL peptide. **c**, Serum samples were collected and assayed by enzyme-linked immunosorbent assay (ELISA) for anti-OVA IgG (day 34). **d**, Mice were immunized on day 0 and day 14 with 1.24 nmol lipo-G_2-CpG mixed with 10 μg SIV Gag protein, blood samples were collected and analysed by peptide-MHC tetramer staining for CD8$^+$ T cells recognizing the immunodominant AL11 epitope of Gag. **e**, **f**, Anti-MSA and anti-OVA IgG (**e**, day 20) or IgM (**f**, day 20) were measured by ELISA. **g**, Groups of C57BL/6 mice ($n = 4$ per group) were immunized with 10 μg OVA alone or mixed with 1.24 nmol of a non-TLR agonist lipo-GpC, the same diacyl lipid tail conjugated to PEG (lipo-PEG, 48 EG units), or DSPE-PEG_{2000}. Mice were boosted with the same formulation on day 14, and OVA tetramer$^+$ CD8$^+$ T cells in peripheral blood were assayed by flow cytometry on day 20. ***$P < 0.001$. **h**, TLR2 knockout or wild-type mice were immunized as described in **a**, and OVA tetramer$^+$ CD8$^+$ T cells were assayed as previously. All data are mean ± s.e.m. *$P < 0.05$. Statistical analysis was performed by unpaired Student's *t*-test.

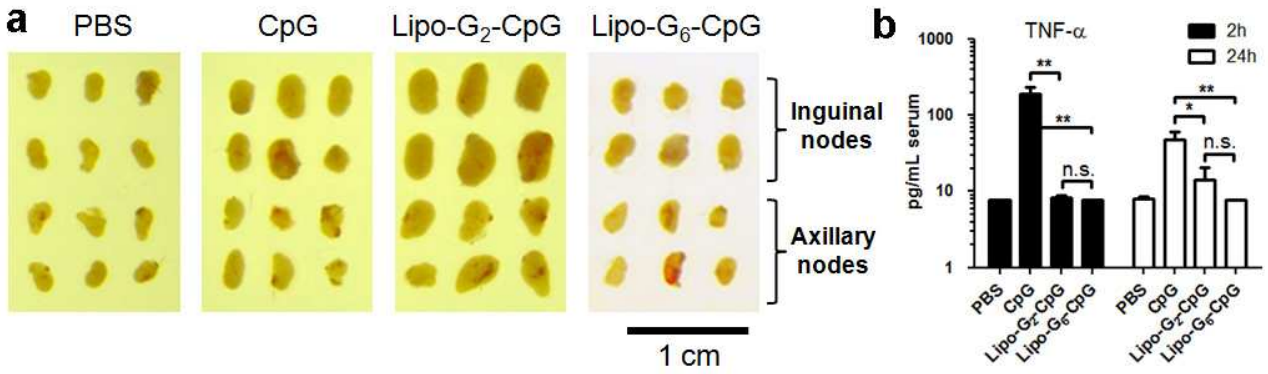

Extended Data Figure 7 | Albumin-binding CpG induces local lymphadenopathy but reduces systemic toxicity compared with soluble CpG adjuvant. **a**, C57BL/6 mice ($n = 3$ per group) were injected with 1.24 nmol CpGs subcutaneously on day 0 and 2.48 nmol CpGs on days 2 and 4. On day 6 mice were killed and LNs were isolated and photographed with a digital camera. **b**, Bead-based flow analysis of proinflammatory cytokines elicited in peripheral blood of mice injected with a single dose (6.2 nmol) of different CpG formulations. Blood samples were collected at different time intervals and analysed for TNF-α, as per manufacturer's instructions. All data are mean ± s.e.m. $^{**}P < 0.01$, $^{*}P < 0.05$. Statistical analysis was performed by one-way ANOVA with Bonferroni post-test.

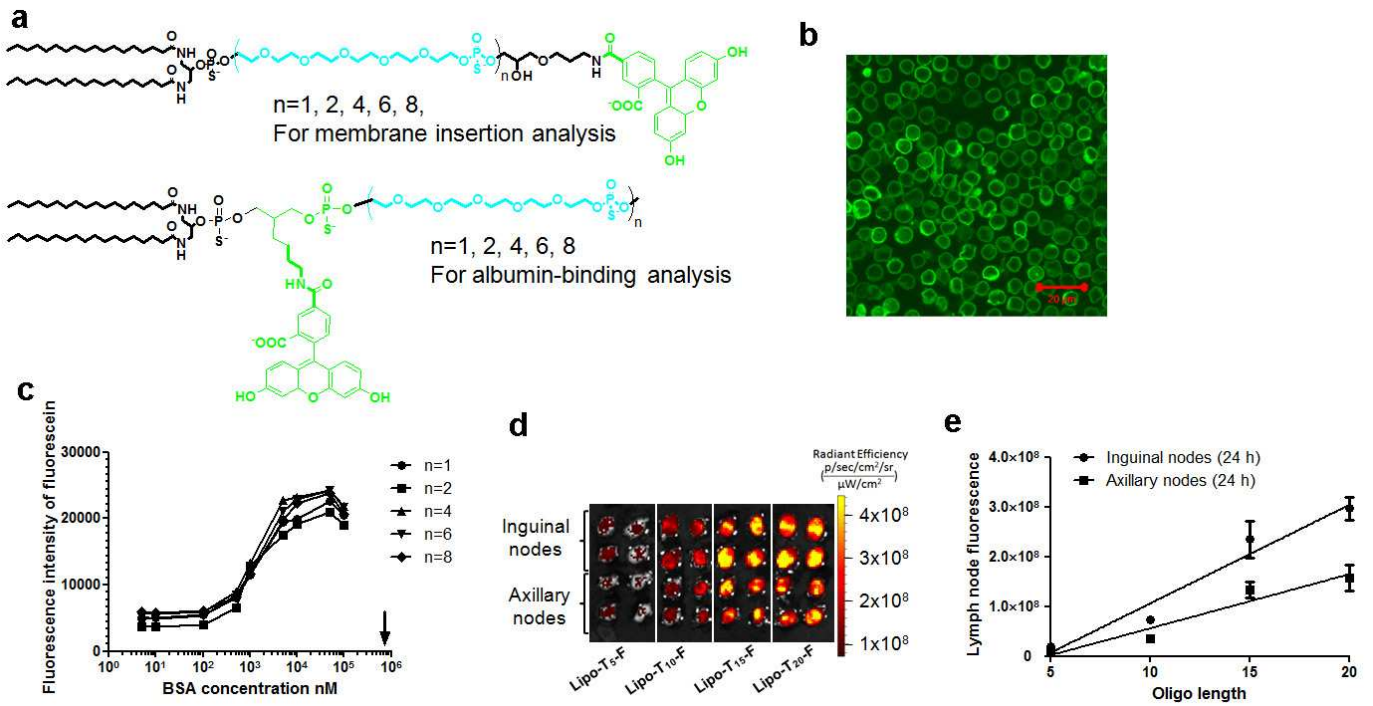

Extended Data Figure 8 | Hydrophilic block length of amphiphiles determines cell membrane insertion and LN accumulation. **a**, Amphiphiles with varying hydrophilic PEG lengths were prepared by solid phase synthesis of diacyl tails coupled to 1–8 hexa-ethylene glycol phosphorothioate units. Fluorescein was incorporated either at the 3′ terminal (for membrane insertion analyses) or adjacent to the lipid moiety (for albumin-binding analyses). **b**, Splenocytes from C57BL/6 mice (5×10^7cells per ml) were incubated with lipo-$(PEG)_n$-fluorescein (1.67 μM) and albumin (100 μM) at 37 °C for 1 h. Shown is a representative image of membrane insertion observed by confocal microcopy for lipo-$(PEG)_1$-fluorescein. **c**, Equilibrium partitioning measurements shown as a function of albumin concentration at 37 °C. Lipo-fluorescein-$(PEG)_n$ (5 μM) was incubated with varying concentrations of BSA and fluorescence intensities were monitored by fluorescence spectroscopy. BSA binding disrupted the micellar structure and decreased the self-quenching of fluorescein. All samples reached maximum fluorescence intensities at around 10 μM BSA, indicating 100% micelle breakup at this concentration (at higher BSA concentrations, fluorescence decreases due to solution turbidity). Arrow indicates plasma concentration of albumin. **d**, **e**, Lipo-T_n-FAM amphiphiles (n = 5, 10, 15, 20) were injected subcutaneously in C57BL/6 mice (n = 4 LNs per group), and excised LNs were imaged after 24 h (**d**). Mean LN fluorescence from groups of mice are plotted in **e**. All data are mean ± s.e.m.

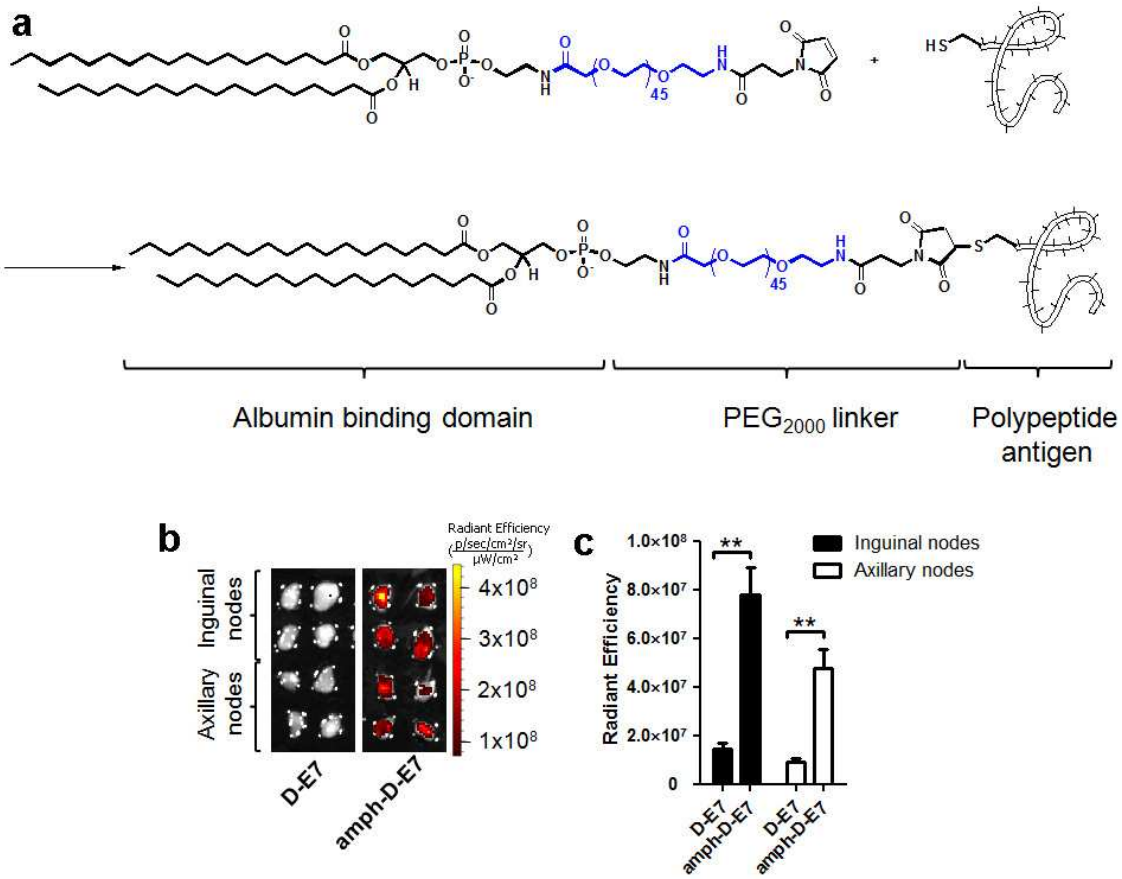

Extended Data Figure 9 | Lipo-PEG-peptide amphiphiles exhibit greatly enhanced LN accumulation compared with unmodified peptides. **a**, Peptides with amino-terminal cysteines were conjugated to maleimide-PEG_{2000}-DSPE. **b**, **c**, FAM-labelled immunodominant peptide derived from the HPV-16 E7 protein (FAM-FTVINYHARC, synthesized in reverse sequence order using D-amino acids to obtain the same chiral organization of side chains as the typical L-amino acid sequence in a protease-resistant peptide) was injected subcutaneously at the tail base as a free peptide (D-E7) or as a PEG-DSPE conjugate (amph-D-E7). Shown are IVIS images of draining LNs 24 h after injection (**b**) and fluorescence quantifications (**c**). All data are mean ± s.e.m. $^{**}P < 0.01$. Statistical analysis was performed by unpaired Student's *t*-test.

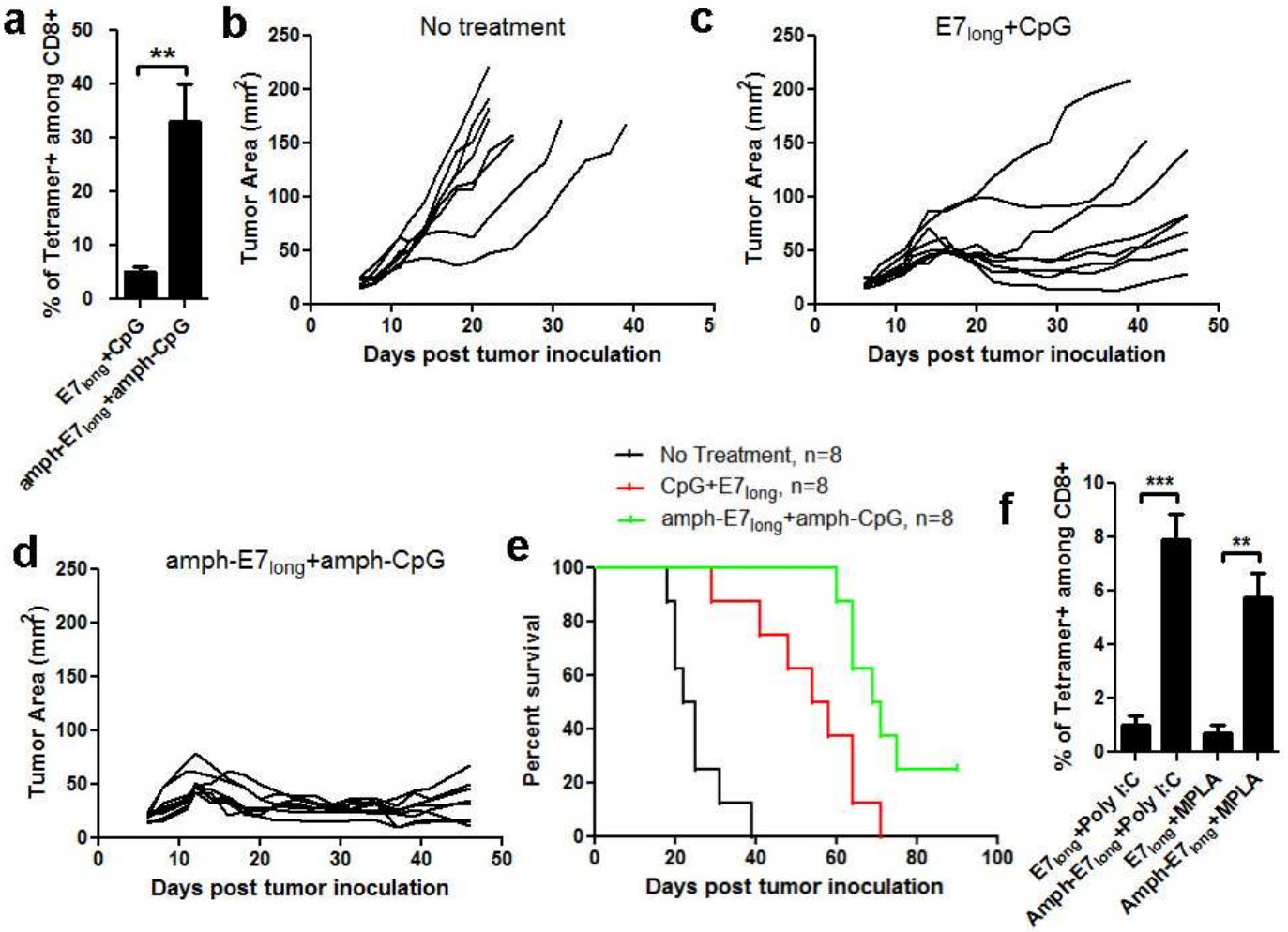

Extended Data Figure 10 | Long-peptide amphiphiles, when combined with amph-CpG, elicit a potent antigen-specific CD8$^+$ T-cell response with therapeutic benefits, as compared to soluble formulation. **a**, C57BL/6 mice were primed on day 0 and boosted on day 14 with amph-E7$_{long}$ (HPV-16 E7$_{43–62,}$ 10 μg peptide) and amph-CpG (lipo-G$_2$-CpG, 1.24 nmol), or equivalent soluble peptide/CpG vaccines. Six days after the boost, mice were bled and analysed for tetramer-positive CD8$^+$ T cells in peripheral blood. **b–e**, C57BL/6 mice ($n = 8$ per group) were inoculated with 3×10^5 TC-1 tumour cells subcutaneously in the flank and left untreated or immunized with soluble or amphiphile long-peptide vaccines on days 6 (10 μg peptide, 1.24 nmol CpG), 13 (20 μg peptide, 1.24 nmol CpG) and 19 (20 μg peptide, 1.24 nmol CpG). **b–d**, Shown are individual tumour growth curves for no treatment (**b**), immunization with soluble E7$_{long}$ and CpG (**c**), or immunization with amph-E7$_{long}$ plus amph-CpG (**d**). Kaplan–Meier survival curves of eight mice per group are shown in **e**. **f**, Long-peptide amphiphiles also elicit potent immune responses when combined with non-CpG, non-LN-targeting alternative adjuvants. C57BL/6 mice ($n = 4$ per group) were immunized as before, using amph-E7$_{long}$ peptide (10 μg) combined with monophosphoryl lipid A (MPLA, 10 μg) or polyinosinic:polycytidylic acid (poly I:C, 50 μg). The frequencies of E7 tetramer$^+$ CD8$^+$ T cells in peripheral blood were assayed on day 20. All data are mean ± s.e.m. $^{***}P < 0.001$, $^{**}P < 0.01$, $^{*}P < 0.05$ by unpaired Student's *t*-test.